

# Design of a reliable numerical model of a plastic scintillation detector for beta spectrometry

L. Fleres<sup>1\*</sup>, J. Venara<sup>1</sup>, M. Cuozzo<sup>1</sup>, C. Mahe<sup>1</sup>, S. Fargier<sup>1</sup>, E. El Haber<sup>1</sup>, F. Carrel<sup>2</sup>

<sup>1</sup>CEA, DES, ISEC, DPME, SEIP, LNPA, Univ. Montpellier, Marcoule, F-30207 Bagnols-sur-Cèze Cedex, France

<sup>2</sup>Université Paris-Saclay, CEA, List, F-91120, Palaiseau, France

(\*) [lorenzo.fleres@cea.fr](mailto:lorenzo.fleres@cea.fr)

**Abstract**— The accurate measurement of beta emitters is of utmost importance in various fields, including environmental monitoring, radiation protection and dismantling and decommissioning (D&D) operations. Non-destructive measurement techniques are crucial as they enable assessments of radioactivity without causing further harm or releasing additional hazardous materials. Due to the limited range of beta particles in matter, their characterization requires measurements in contact with the source term. In this paper, we present a study on the performance evaluation of a plastic scintillation detector designed for *in-situ* beta spectrometry measurements. The MCNP6.2 numerical model of the detector is detailed in the measurement configuration with beta, gamma and internal conversion electrons emitting sources. The calibration process and Gaussian Energy Broadening (GEB) parameters evaluation are discussed. Comparisons between the MCNP6.2 simulations and experimental measurements are exposed, both for gamma and beta spectra. While the gamma-ray detector response shows good agreement, greater discrepancies are observed in the beta ray response. To shed light on these discrepancies, a sensitivity analysis considering various sources of uncertainties is planned for future work.

**Keywords** — Beta spectrometry, Gaussian energy broadening, Monte Carlo, Plastic scintillator.

## I. INTRODUCTION

THE characterization of pure beta emitting radionuclides is difficult due to the very short path of electrons in matter. Their detection is usually performed in laboratory conditions by destructive analysis. Liquid scintillation counting, is still the reference method for characterizing pure beta emitters but requires numerous upstream operations [1]. These operations are often time-consuming and entail specific constraints in terms of safety and security. Additionally to destructive techniques, *in situ* measurement methods can be used to obtain initial knowledge of the radiological state of the materials to be characterized [2]–[5]. Plastic scintillators are currently the best candidates for *in situ* beta particle detection as they have the lowest density and effective atomic number of all solid scintillators. These properties make them less sensitive to gamma radiation thus enhancing the ratio of beta signal to gamma background, which is always present during *in situ*

measurements.

In previous works, CEA has developed a methodology based on a portable beta plastic scintillator spectrometer for *in situ* radiological characterization of <sup>90</sup>Sr in contaminated matrices [5]. We plan to use this methodology for the *in situ* characterization of beta emitting radionuclide mixtures using deconvolution techniques. This requires performing numerical simulations to obtain an accurate response function of the detector for different radionuclides and measurement configurations.

In this study, beta and gamma responses of the plastic scintillator were evaluated using MCNP6.2 [6] simulations and compared with laboratory measurements. In section II, we describe the measurement methodology, the numerical model of the detector and the method used for the energy calibration and energy resolution computation. In section III, the results and the comparison between measurements and MCNP6.2 simulations for two standard sources of <sup>137</sup>Cs and <sup>207</sup>Pb are provided. In section IV, we summarize the key findings of the study and outline potential areas for further research and improvements.

## II. MATERIALS AND METHODS

### *A Measurement methodology*

The plastic scintillation detector for beta spectrometry was designed in previous work [5]. The sensitive part of the detector consists of a 4 mm thick EJ200 scintillator with an 18 micrometer Mylar window used to avoid ambient light sensitivity. A 30 mm thick Poly(methyl methacrylate) (PMMA) light guide couples the scintillator to the photocathode of a photomultiplier. For data acquisition and analysis, the probe is connected via a LYNX multichannel analyzer (MIRION Technologies, CA, USA) to a computer equipped with the Genie 2000 software [7]. Fig. 1 shows the experimental set-up. The measurement methodology requires to perform two measurements [4], [5], [8]: a first one with the bare detector and a second one with a 4 mm thick aluminum cover placed over the detector. This cover was designed to stop energetic beta particles up to 2.3 MeV and to ensure that the detector only measures gamma rays if exposed to <sup>90</sup>Sr/<sup>90</sup>Y contaminated environment. The subtraction of the two acquired spectra provides the beta component as shown in Fig. 2, which illustrates the spectra acquired for a <sup>137</sup>Cs source. The blue line represents the response of the detector to the photons emitted

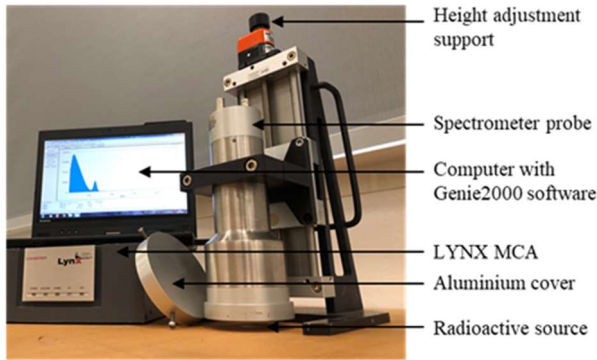


Fig. 1. Beta spectrometry probe and instrumentation devices.

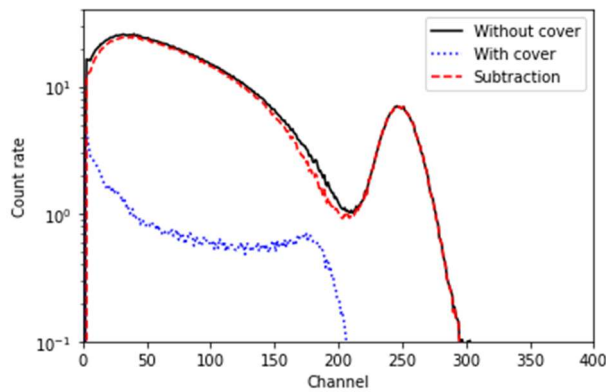


Fig. 2. Measured spectra for a  $^{137}\text{Cs}$  source placed at a distance of 1 cm from the detector.

by the  $^{137}\text{Cs}$  source. The photons emitted at 661.66 keV mainly interact by Compton scattering and the resulting spectrum has no full absorption peak. The red line, obtained by subtraction of the two measurements, is a convolution of the continuous  $\beta$ -component and the peak arising from the internal conversion electrons emitted at energies of 624.22 and 655.67 keV. The poor energy resolution of the detector does not allow to discriminate the two peaks.

### B MCNP6.2 numerical model

In previous studies [5], the MCNP6.1 code was used to create a numerical model of the beta spectrometry detector. We updated the model for MCNP version 6.2 and changed the design of the calibration source since we have used a different set-up. We procured new radioactive sources from the Electron Sources Series of Eckert & Ziegler [9]. These sources are prepared by evaporation of the radionuclide on very thin surface foil, and protected by a 100-200  $\mu\text{g}\cdot\text{cm}^{-2}$  acrylic cover. The source modelling was based on the geometric characteristics available in the product catalog. The source term was assumed to be homogeneously distributed in a cylinder of air of a very small thickness (0.1  $\mu\text{m}$ ) placed between the substrate and the acrylic window. Fig. 3 shows the numerical model with the calibration source placed at a distance of 10 mm from the detector.

In this work we used a  $^{137}\text{Cs}$ , a  $^{207}\text{Bi}$  and a  $^{241}\text{Am}$  gamma ray source. The characteristics of the sources are summarized in Table I in which square brackets indicate the emission intensities.

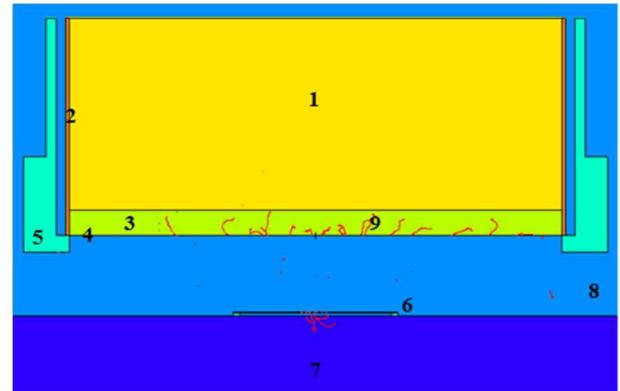


Fig. 3. MCNP6.2 model of measurement configuration. (1) PMMA light guide, (2) Polytetrafluoroethylene (PTFE) reflector, (3) EJ200 scintillator, (4) Mylar window, (5) aluminium case, (6) calibration point, (7) concrete floor, (8) ambient air, (9) 1 MeV electron collision point.

Emission data for different radionuclides were taken from the Joint Evaluated Fission and Fusion (JEFF) nuclear data library version 3.3 [10] except for  $\beta$ - emissions. For the latter, we considered data from the BetaShape program [11] in order to take into account experimental shape factors of beta emitters.

The numerical model allows to assess the performance of the detector and to compare with experimental results. To obtain the energy distribution of pulses in the sensitive part of the detector we applied a “F8” pulse height tally to the cell representing the EJ200 material. The MCNP code assumes that the detector is ideal and does not consider all the physical processes that determine its energy resolution. To take account of the statistical dispersion in MCNP simulations, the GEB (Gaussian Energy Broadening) option must be activated in MCNP for the F8 tally. The function relating the detector's energy resolution ( $FWHM$  – full width at half maximum) to a given energy ( $E$ ) is expressed as follows:

$$FWHM(E) = a + b\sqrt{E} + c \times E^2, \quad (1)$$

The procedure for evaluating parameters  $a$ ,  $b$  and  $c$  will be presented in section II.C.

We used the default parameters for photon and electron transport (PE mode) in all simulations.

### C Energy calibration and energy resolution of the detector

Following a different approach compared to the previous study [5], we carried out the energy calibration process and energy resolution evaluation according to the response of the detector to gamma sources. The method used is the one proposed by Kim *et al.* [12]. Through an iterative process of Monte Carlo simulations, energy calibration and energy resolution update, convergence is achieved. At the first iteration the calibration is carried out according to the positions of the measured Compton maxima and the energy resolution is evaluated with a Gaussian adjustment on the Compton maxima. From the second iteration onward, the Gaussian adjustment is performed on the position of the Compton edges as shown in Fig. 4 for a  $^{137}\text{Cs}$  source. In the case of the  $^{241}\text{Am}$  source, Gaussian adjustment was performed on the full absorption peak resulting from the 59.5 keV gamma ray emission. Although for energies greater than 30 keV the Compton effect is prevalent

TABLE I  
CHARACTERISTICS OF CALIBRATION SOURCES

Radionuclide	<sup>137</sup> Cs	<sup>207</sup> Bi	<sup>241</sup> Am
Activity (kBq)	9.07 ± 2.5%	9.37 ± 2.5%	151.0 ± 5.0%
Eckert & Ziegler type	Mono-Energetic Series	Mono-Energetic Series	Alpha Wide Area
Gamma emission (keV)	661.66 [85.05%]	569.70 [97.76%] 1063.66 [74.58%] 481.69 [1.55%] 555.25 [0.43%] 975.66 [7.11%] 1049.20 [1.84%] 1060.49 [0.44%]	59.54 [35.92%]
Discrete electron emission (keV)	624.22 [7.78%] 655.67 [1.70%]	-	-
$\beta$ - transitions (keV)	Forbidden 1 <sup>st</sup> unique: 513.97 [94.61%] Forbidden 2 <sup>nd</sup> non-unique: 1175.63 [5.39%]	-	-

Activities are provided at the measurement date.

Internal conversion electrons emitted by <sup>241</sup>Am are omitted as we are interested only in the gamma response.

EC, electron capture.

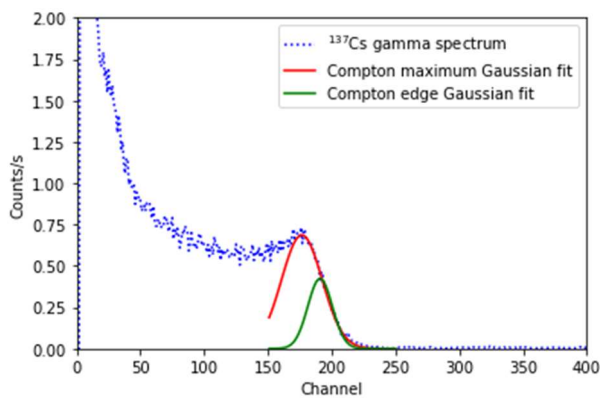


Fig. 4. Gaussian adjustments on the <sup>137</sup>Cs gamma spectrum.

over the photoelectric effect in the EJ200, a full absorption peak is distinguishable in the measured <sup>241</sup>Am spectrum (results are not shown here).

We carried out all the adjustment using the Curve Fitter Toolbox [13] available in MATLAB and the Linear Least Squares method.

### III. RESULTS AND DISCUSSION

#### A Energy calibration and GEB parameters computation

Following the procedure described in section II.C we achieved convergence just after 4 iterations. The resulting energy calibration is:

$$\text{Energy (MeV)} = 0.014 + 0.00245 \times \text{Channel}, \quad (2)$$

Fig. 5 shows the evolution of the energy resolution curves obtained at each iteration. The dotted points represent the FWHM values evaluated by Gaussian fitting at the energy values of 59.54, 477.34, 393.31 and 857.65 keV. The first value corresponds to the energy of the full absorption peak of <sup>241</sup>Am, the last three values are the theoretical Compton edge [14] energies for photons emitted by <sup>137</sup>Cs and <sup>207</sup>Bi listed in Table I. The values obtained for the *a*, *b* and *c* parameters of the GEB function at each iteration are summarized in Table II.

We compared the obtained results with the evaluation of the energy resolution from the electron response of the detector. We focused on the region between 525 and 725 keV of the <sup>137</sup>Cs beta spectrum, where the signal produced by the internal

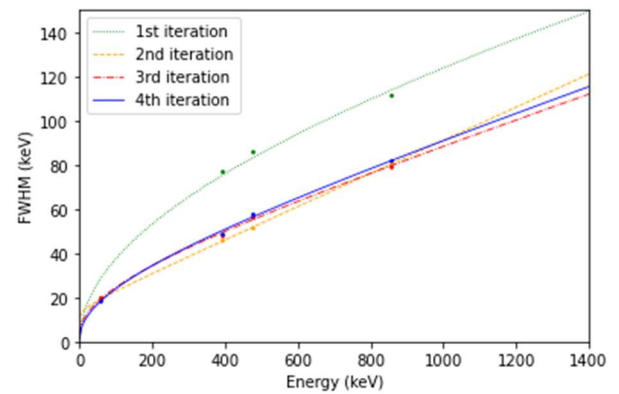


Fig. 5. FWHM curves as a function of the iteration number.

TABLE II  
GEB PARAMETERS AS A FUNCTION OF THE ITERATION NUMBER

Iteration	<i>a</i> (MeV)	<i>b</i> (MeV <sup>-1</sup> )	<i>c</i> (MeV <sup>-1</sup> )
1	0.0003	0.1171	0.1135
2	0.012	0.0289	6.69
3	0.0033	0.065	0.7131
4	0.0011	0.0702	0.6385

conversion electrons is dominant. In this range, the total response is given by the convolution of three components. The first is a continuous component associated with the  $\beta$ - emission. The second and third are the two components associated with the two internal conversion electrons. We then defined a custom function to perform a deconvolution as the sum of a linear component and two Gaussians of relative amplitudes equal to the emission ratio of the internal conversion electrons. The result of deconvolution is shown in Fig. 6. The FWHM values obtained are 66.63 keV and 69.60 keV for the two Gaussians centered at 620.12 and 652.36 keV, respectively. Calculating the FWHM values for the energies of 620.12 and 652.36 keV based on equation (1) with the obtained *a*, *b* and *c* parameters given in Table II results in 66.64 keV and 68.56 keV. The relative error of less than 1.5% supports our energy calibration and energy resolution evaluation process based on gamma ray sources.

An evaluation of the energy resolution can be obtained using the internal conversion peaks around 975 keV of the <sup>207</sup>Bi source but the presence of three internal conversion electrons

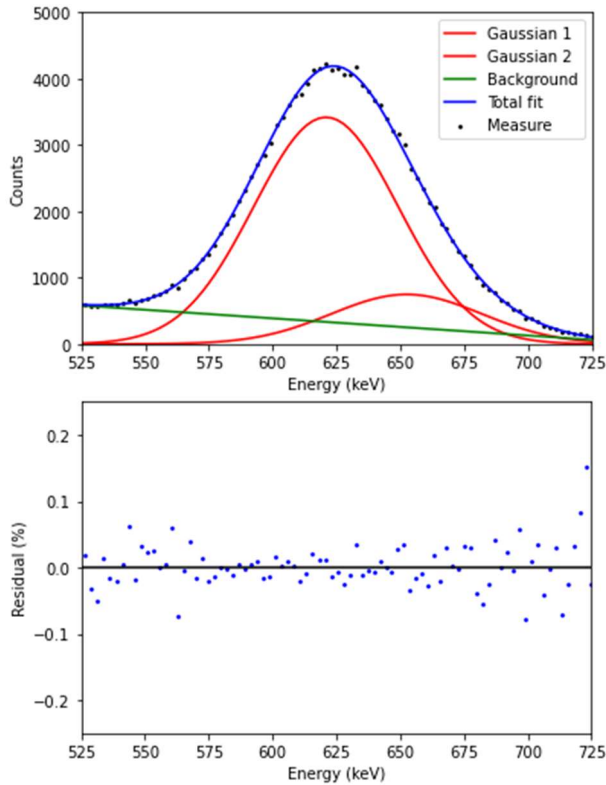


Fig. 6. (a) The analysis of  $^{137}\text{Cs}$  beta spectrum in the region of the internal conversion peak. The peak is fitted with two Gaussian functions (red) and a linear background (green). (b) Residuals expressed in percentage between measurement and adjustment.

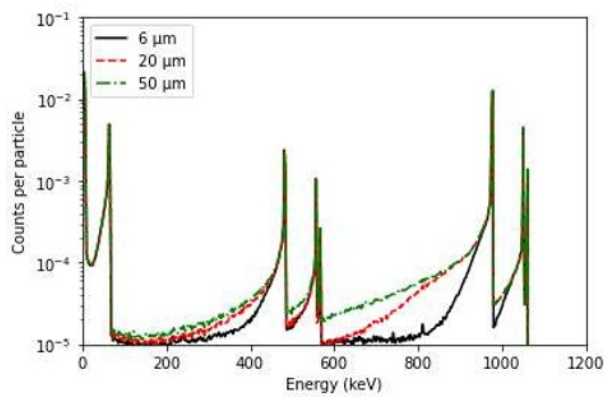


Fig. 7. Electron energy flux coming from the  $^{207}\text{Bi}$  source as a function of platinum substrate thickness. Results obtained using an F1-type tally in MCNP6.2.

makes deconvolution more complex. Moreover, compared to the  $^{137}\text{Cs}$  source where the substrate is a thin Mylar foil, the  $^{207}\text{Bi}$  source substrate is made of platinum. Such a high-density and high atomic number material strongly impacts the backscattering and self-absorption of electrons in the source, as well as the production of Bremsstrahlung photons. The impact of the platinum thickness on the electron flux leaving the source is shown in Fig 7. To obtain a correct estimate of the resolution based on the detector response to a  $^{207}\text{Bi}$  source, a high-quality source must be used in order to limit the emission spectrum degradation.

### B Comparison of MCNP6.2 simulations and measurements

The comparison between experimental measurements and Monte Carlo simulations is the last step in the qualification phase of a detector numerical model. We used the activity value of the various sources under  $4\pi$  at the measurement date as the multiplication factor to compare simulated and measured responses. The previously obtained energy calibration and GEB function were applied to F8-tally for all the simulations. The spectra for  $^{137}\text{Cs}$  and  $^{207}\text{Bi}$  sources are shown in Fig. 8: gamma ray spectra represent the measurement with the cover and beta spectra are obtained as the subtraction of the two measurements (without and with the cover).

A qualitative analysis shows good agreement between simulated and measured gamma spectra. In the MCNP numerical model, the aluminium cover was added on the detector to take into account the attenuation and build-up of photons in the cover itself. Regarding the beta spectra, the shape of the  $^{137}\text{Cs}$  spectrum appears to be accurately rebuilt in the region of the internal conversion emission with a larger gap at low energy (50 – 500 keV). On the other hand, looking at the spectrum of  $^{207}\text{Bi}$ , the gap between simulation and measurement is important, again in the lower energy region but especially in the region of the internal conversion peak around 975 keV. The largest deviation for the  $^{207}\text{Bi}$  simulation is associated with the uncertainty related to the platinum substrate on which the radionuclide is deposited.

The quantitative analysis was carried out by comparing the integrated counts over different energy intervals, focusing on the global spectra and the internal conversion electrons emission regions. The relative deviations between measured and simulated counts for  $^{137}\text{Cs}$  and  $^{207}\text{Bi}$  sources are listed in Table III. For the total spectrum electron responses, we considered a low energy threshold at 50 keV for  $^{137}\text{Cs}$  and 100 keV for  $^{207}\text{Bi}$ . Below these energies, the attenuation of X-rays emitted by the sources during the two measurements must be taken into account. The relative deviations of gamma responses are lower than 2% which confirms the reliability of the detector to the measurement of gamma-emitting radionuclides. Larger differences are encountered for the electron responses with a 22% maximum deviation for  $^{207}\text{Bi}$ .

The discrepancy between Monte Carlo simulations and  $\beta$ -spectra measurements may be due to several factors. Among the most important of which are: the algorithm and physical electron transport parameters, the modelling and quality of the source, the nuclear radionuclide emission data and the cross-

TABLE III  
COMPARISON OF THE MEASURED AND SIMULATED SPECTRA OF THE CALIBRATION SOURCES.

Radionuclide	Response	Energy range (keV)	Relative deviation { S/M - 1 }
$^{137}\text{Cs}$	$\gamma$ <sup>(a)</sup>	50 – 700	+0.0
	$e^-$ <sup>(a)</sup>	50 – 1200	+11.0
	$e^-$ <sup>(b)</sup>	525 – 725	+8.0
$^{207}\text{Bi}$	$\gamma$ <sup>(a)</sup>	40 – 1100	+1.8
	$e^-$ <sup>(a)</sup>	100 - 1300	+2.0
	$e^-$ <sup>(b)</sup>	400 – 600	-6.7
	$e^-$ <sup>(c)</sup>	850 – 1200	+21.7

<sup>(a)</sup> Total spectrum. <sup>(b)</sup> Internal conversion 1st peak. <sup>(c)</sup> Internal conversion 2nd peak.

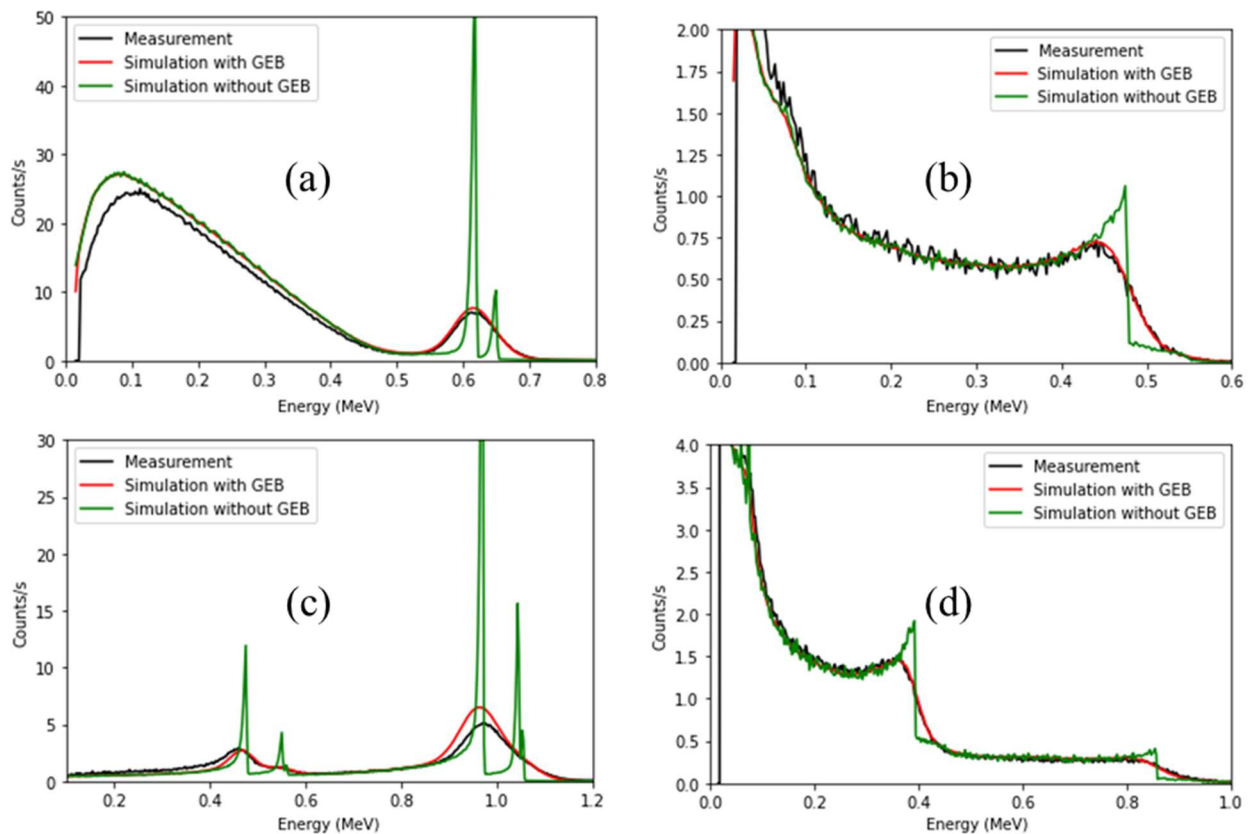


Fig. 8. Comparison of the measured (black) and simulated spectra with Gaussian energy broadening (red) and without (green) : (a)  $^{137}\text{Cs}$  beta contribution, (b)  $^{137}\text{Cs}$  gamma contribution, (c)  $^{207}\text{Bi}$  beta contribution, (d)  $^{207}\text{Bi}$  gamma contribution.

sections used in our simulations. We plan to carry out in future works a detailed sensitivity analysis to assess the impact of different sources of uncertainties on our numerical detector model.

#### IV. CONCLUSIONS

In this study, we assessed the performance of a plastic scintillation detector to measure gamma radiation and beta particles. Comparison between Monte Carlo simulations using MCNP6.2 and laboratory measurements showed good agreement for the gamma-ray detector response. Regarding the detector response to electrons, we still encountered significant discrepancies between measurements and simulations. These deviations will be investigated in the future by means of an in-depth parametric analysis and by comparison of Monte Carlo numerical models using independent Monte Carlo codes. The conclusions of this study contribute to the understanding of the plastic scintillation detector's capabilities and limitations and pave the way for further improvements in the numerical modeling of this type of detector.

#### REFERENCES

[1] K. A. Arslanov, T. V. Tertychnaya, and S. B. Chernov, 'Problems and Methods of Dating Low-Activity Samples by Liquid Scintillation Counting', *Radiocarbon*, vol. 35, no. 3, pp. 393–398, Jan. 1993, doi: 10.1017/S0033822200060409.

[2] A. Schilk, K. H. Abel, D. Brown, R. Thompson, M. Knopf, and C. Hubbard, 'Selective, high-energy beta scintillation sensor for real-time, in situ characterization of uranium-238 and strontium-90', 1995, doi: 10.1007/BF02041923.

[3] B.-K. Seo, C.-H. Park, K.-W. Lee, D.-G. Lee, and C.-H. Jung, 'Development of the In-situ Monitoring System for Pipe Internal Contamination Measurement in the Decommissioning Site', *Journal of Nuclear Science and Technology*, vol. 45, pp. 500–502, Aug. 2014, doi: 10.1080/00223131.2008.10875900.

[4] V. Potapov, A. G. Volkovich, O. Ivanov, V. Stepanov, S. Smirnov, and V. G. Volkov, 'Development of Portable Beta Spectrometer for Sr-90 Activity Measurements in Field Conditions and Its Application in Rehabilitation Activities at RRC Kurchatov Institute', *undefined*, 2006, Accessed: Jan. 27, 2022. [Online]. Available: <https://www.semanticscholar.org/paper/Development-of-Portable-Beta-Spectrometer-for-Sr-90-Potapov-Volkovich/57324a32fe9a3543ba592526ce7de536f0bbd4fd>

[5] J. Venara *et al.*, 'Design and development of a portable  $\beta$ -spectrometer for  $^{90}\text{Sr}$  activity measurements in contaminated matrices', *Nuclear Instruments and Methods in Physics Research Section A: Accelerators, Spectrometers, Detectors and Associated Equipment*, vol. 953, p. 163081, Feb. 2020, doi: 10.1016/j.nima.2019.163081.

- [6] C. J. Werner *et al.*, ‘MCNP Version 6.2 Release Notes’, LA-UR--18-20808, 1419730, Feb. 2018. doi: 10.2172/1419730.
- [7] Z. Laili, ‘Genie TM 2000 spectroscopy software operations, Canberra 52 (1) (2016) 1–361.’, 2016.
- [8] D. E. Martz, B. L. Rich, and L. O. Johnson, ‘A Portable Beta Spectrometer for Tissue Dose Measurement’, *Radiation Protection Dosimetry*, vol. 14, no. 2, pp. 183–186, Feb. 1986, doi: 10.1093/oxfordjournals.rpd.a079644.
- [9] ‘Eckert & Ziegler Strahlen- und Medizintechnik AG’, *Eckert & Ziegler Strahlen- und Medizintechnik AG*, Jun. 17, 2022. <https://www.ezag.com/home/> (accessed Jun. 24, 2022).
- [10] A. J. M. Plompen *et al.*, ‘The joint evaluated fission and fusion nuclear data library, JEFF-3.3’, *The European Physical Journal A*, vol. 56, no. 7, p. 181, Jul. 2020, doi: 10.1140/epja/s10050-020-00141-9.
- [11] X. Mougeot, ‘BetaShape: A new code for improved analytical calculations of beta spectra’, *EPJ Web Conf.*, vol. 146, p. 12015, 2017, doi: 10.1051/epjconf/201714612015.
- [12] C. Kim, Y. Kim, M. Moon, and G. Cho, ‘Iterative Monte Carlo simulation with the Compton kinematics-based GEB in a plastic scintillation detector’, *Nuclear Instruments and Methods in Physics Research Section A: Accelerators, Spectrometers, Detectors and Associated Equipment*, vol. 795, pp. 298–304, Sep. 2015, doi: 10.1016/j.nima.2015.06.007.
- [13] ‘Curve Fitting Toolbox’. <https://www.mathworks.com/products/curvefitting.html> (accessed Aug. 07, 2023).
- [14] C. L. Fontana, ‘Compton edge calculator’, *Cristiano Lino Fontana*, Mar. 16, 2018. <https://userswww.pd.infn.it/~moretto/fontana/project/software/2018/03/16/fontana/project/software/2018/03/16/compton-edge.html> (accessed Jul. 31, 2022).